EPJ Web of Conferences **142**, 01009 (2017) DOI: 10.1051/epjconf/201714201009
Advances in Dark Matter and Particle Physics

Dark Searches and $\gamma\gamma$ Physics at KLOE

Francesca Curciarello on behalf of the KLOE-2 Collaboration[1,a]

[1] *Laboratori Nazionali di Frascati, 00044, Frascati, Italy*

Abstract. The search for a dark sector mediated by a new gauge boson, the dark photon, is motivated by many astrophysical anomalies and by the $g-2$ discrepancy. The KLOE experiment, operating at the e^+e^- DAΦNE collider in Frascati, searched for a visibly-decaying dark photon by investigating the ϕ-Dalitz decay into the η meson, the dark photon production from continuum, and the Higgsstrahlung process. The KLOE-2 run started in November 2014, after the upgrade of both, DAΦNE and the KLOE apparatus. In particular, two high electron and positron tagger stations were installed in the DAΦNE layout to study $\gamma\gamma$ interactions at 1 GeV. Progress status of the project is given.

1 Introduction

One of the unsolved problems in modern physics is represented by the dark matter (DM). As for visible matter the only way to gain insights into the DM particle nature is to make it interact with baryonic matter. For this reason the hypothesis of a new interaction, dubbed as dark force, between DM and Standard Model (SM) particles, has motivated a great world-wide experimental effort, mostly regarding recent puzzling astrophysical and terrestrial anomalies [6–12]. The dark force should be carried by a new light (<1 GeV) boson messenger [1] with a very weak coupling defined as the ratio of effective dark and fine structure coupling constants, $\varepsilon^2 = \alpha'/\alpha \ll 1$ [1–5]. Moreover, the dark photon should get mass by means of a Higgs-like mechanism which implies the existence of at least one additional scalar particle, the dark Higgs h′. Dark photon search is also strongly motivated since it would give a positive one-loop contribution to the calculated value of the muon magnetic moment anomaly, a_μ, thus explaining the observed discrepancy with the experimental value, for dark photon masses of 10–100 MeV and coupling constant ε of about 10^{-3} [13]. In this paper, we present a review of all KLOE results on visibly-decaying dark photon, obtained by analysing data of the first KLOE run (2000-2006).

A new run, KLOE-2, has started in November 2014 with an upgraded DAΦNE and KLOE detector. One of the main goal of KLOE-2 is the precision measurement of the π^0 width, $\Gamma_{\pi^0\to\gamma\gamma}$, which is considered a strong test of low-energy QCD. The $\Gamma_{\pi^0\to\gamma\gamma}$ is predicted with 1.4% of precision ($\Gamma^{\rm Th.}_{\pi^0\to\gamma\gamma} = 8.09 \pm 0.11$eV [14, 15]) while the world average experimental value is known with 6% precision ($\Gamma^{\rm PDG}_{\pi^0\to\gamma\gamma} = 7.74 \pm 0.48$eV [16]), dominated by the discrepancy between the most sensitive measurements, the direct one and that obtained with the Primakoff conversion [17]. A way to achieve the precision needed to test QCD predictions is to study the π^0 production through $\gamma\gamma$ fusion in the $e^+e^- \to e^+e^-\gamma^\star\gamma^\star \to e^+e^-\pi^0$ reaction. This purpose could be achieved by KLOE-2 thanks to the installation, in both arms of the DAΦNE layout, of two tagger stations in order to tag high energy scattered electron and positrons coming from $\gamma\gamma$ interactions. About 10^4 events are expected at KLOE-2 with an integrated luminosity of 5 fb^{-1} [18].

KLOE-2 aims also to perform the first measurement of the $F_{\pi^0\gamma^*\gamma}$ form factor at low $Q^2 \le 0.1\,\mathrm{GeV}^2$ in the space-like region. This measurement can have an impact on the value and precision of the contribution of one-neutral pion exchange to the hadronic light-by-light scattering, $a_\mu^{\mathrm{LbyL};\pi^0}$, a term of the muon anomaly, g-2 [18].

Progress and operation status of the $\gamma\gamma$ taggers are reviewed in Sec. 5.

2 DAΦNE collider and KLOE detector

DAΦNE is an e^+e^- collider running at the energy $\sqrt{s} = m_\phi = 1.0195$ GeV located at Laboratori Nazionali di Frascati of INFN. It consists of a linear accelerator, a damping ring, nearly 180 m of transfer lines, and two storage rings that intersect at two points.

The KLOE detector is made up of a large cylindrical drift chamber (DC) [19], surrounded by a lead scintillating fiber electromagnetic calorimeter (EMC) [20]. A superconducting coil around the EMC provides a 0.52 T magnetic field. The calorimeter is divided into a barrel and two end–caps and covers 98% of the solid angle. The modules are read out at both ends by 4880 photo–multipliers. Energy and time resolutions are $\sigma_E/E = 5.7\%/\sqrt{E(\mathrm{GeV})}$ and $\sigma_t = 57\,\mathrm{ps}/\sqrt{E(\mathrm{GeV})} \oplus 100\,\mathrm{ps}$, respectively. The all-stereo drift chamber, $4\,m$ in diameter and $3.3\,m$ long, has a mechanical structure of carbon fiber-epoxy composite

[a] e-mail: Francesca.Curciarello@lnf.infn.it

[1] Referred to also as U, A', γ' or simply dark photon.

© The Authors, published by EDP Sciences. This is an open access article distributed under the terms of the Creative Commons Attribution License 4.0 (http://creativecommons.org/licenses/by/4.0/).

and operates with a light gas mixture (90% helium, 10% isobutane). The position resolutions are $\sigma_{xy} \sim 150\,\mu$m and $\sigma_z \sim 2$ mm. The momentum resolution $\sigma_{p_\perp}/p_\perp$ is better than 0.4% for large angle tracks. Vertices are reconstructed with a spatial resolution of ~ 3 mm.

To allow a better vertex reconstruction near the interaction point (IP), an higher acceptance to low p_t tracks and to increase the tightness of the detector, KLOE has been upgraded with a inner tracker [21] (four layers of triple GEM) and two calorimeters, the CCALT [22], made of LYSO crystals, and the QCALT [22], surrounding the DAΦNE quadrupoles and made of tungsten and plastic scintillator tiles. Moreover, in both arms of the DAΦNE layout two couple of tagger stations have been installed to study $\gamma\gamma$ physics. The low energy tagger (LET) [23], has been installed at 1 m from the IP in order to tag e^+e^- of $160 < E < 400$ MeV, and it is made up of LYSO crystals. The high energy tagger (HET) [24] is a plastic scintillator hodoscope whose energy acceptance is expected from $420 < E < 490$ MeV and has been installed at 11 m from the IP just after the DAΦNE bending dipoles.

3 Dark forces

The KLOE Collaboration searched for dark photon signature by investigating three processes and six different channels. In Fig. 1 all limits set by KLOE are reported in comparison with all other constraints in the 0-1 GeV mass range. In the next sections all the analyses performed to extract the KLOE limits are described.

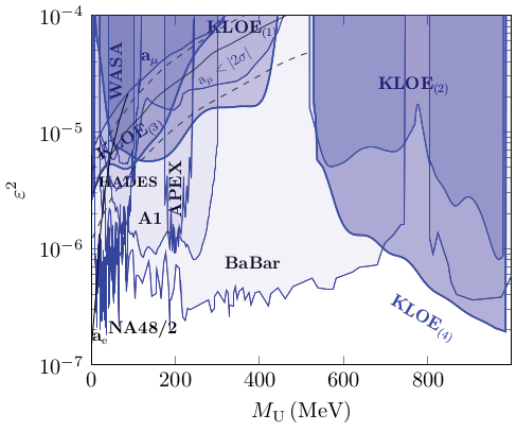

Figure 1. 90% CL exclusion plot for ε^2 as a function of the U-boson mass. The limits from the A1 [25] and APEX [26] fixed-target experiments, the limits from the ϕ Dalitz dacay ($KLOE_{(1)}$) [27, 28] and $e^+e^- \to U\gamma$, $U \to \mu^+\mu^-$, e^+e^-, $\pi^+\pi^-$ ($KLOE_{(2)}$, $KLOE_{(3)}$ and $KLOE_{(4)}$ respectively) [29–31], the WASA [32], HADES [33], BaBar [34] and NA48/2 [35] limits are shown. The solid lines are the limits from the muon and electron anomaly [13]. The gray line shows the U boson parameters that could explain the discrepancy between SM prediction and the experimental value of muon anomaly, a_μ, with a $2\,\sigma$ error band (gray dashed lines) [13].

3.1 ϕ-Dalitz decay

The dark photon is expected to be produced in vector to pseudoscalar meson decays with a rate ε^2 times suppressed with respect to the ordinary transitions [36], producing a peak in the invariant mass distribution of the electron-positron pair over the continuum Dalitz background.

The KLOE Collaboration set a constraint on the U-boson coupling ε^2, by exploiting the $\phi \to \eta e^+e^-$ decay, where the η meson is tagged by $\pi^+\pi^-\pi^0$ [27] and $3\pi^0$ decays [28]. The first analysis used a data sample of 1.5 fb^{-1} of integrated luminosity. The limit on the number of U-boson events has been set by using the Confidence Level Signal (CL_S) technique [37–39]. This first upper limit (UL) has been then updated, improving sample statistics and background rejection (2% of background contamination), and combined with a new limit derived by tagging the η meson by its neutral decay into $3\pi^0$ [28]. For this new analysis, 30577 events are selected from a data sample of 1.7 fb^{-1} with 3% of residual background. For each channel, the irreducible background is extracted directly by a fit to data (see red line in Fig. 2) excluding for each U-boson mass hypothesis the signal region used for the upper limit evaluation (5 MeV centred around m_U). A

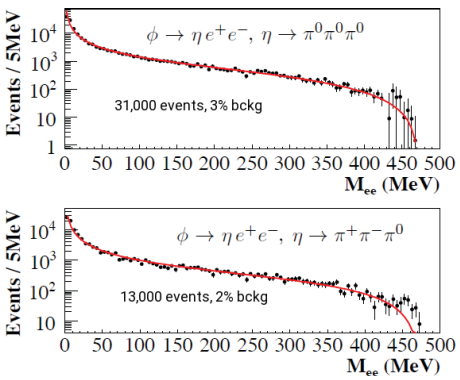

Figure 2. M_{ee} spectrum for the Dalitz decay $\phi \to \eta e^+e^-$, with $\eta \to \pi^0\pi^0\pi^0$ (top) and $\eta \to \pi^+\pi^-\pi^0$ (bottom), red line is a fit to the distribution.

combined UL on the parameter ε^2 at 90% CL has been derived by using the Vector Meson Dominance expectation for the transition form factor slope ($b_{\phi\eta} \sim 1$ GeV^2) resulting in $\varepsilon^2 < 1.7 \times 10^{-5}$ for $30 < M_U < 400$ MeV, and $\varepsilon^2 < 8.0 \times 10^{-6}$ for the sub-region $50 < M_U < 210$ MeV. The above final combined limit is shown in Fig. 1 and dubbed as $KLOE_{(1)}$. This limit, published in 2013 [28] rules out a wide range of U-boson parameters that could explain the a_μ discrepancy in the hypothesis of visibly-decaying dark photon.

3.2 Uγ events

Radiative U-boson production in $e^+e^- \to U\gamma$, $U \to l^+l^-$, $l = e, \mu, \pi$ events is a very sensitive process, independent of the details of the dark Higgs sector. The U boson

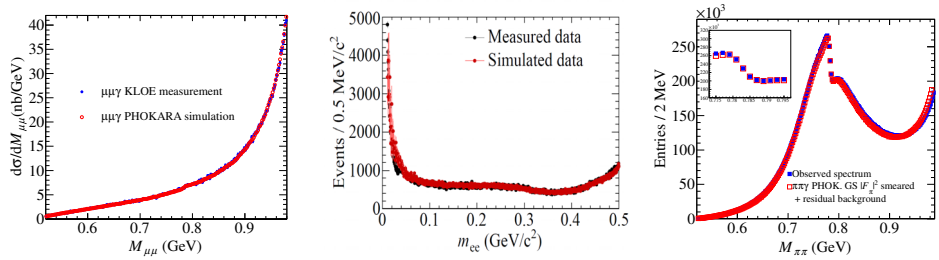

Figure 3. Invariant mass distributions at the end of the analysis selections for the $e^+e^- \to U\gamma$, $U \to \mu^+\mu^+$, e^+e^-, $\pi^+\pi^+$ processes. From left to right: $M_{\mu\mu}$, M_{ee} and $M_{\pi\pi}$ in comparison with expectation from PHOKHARA ($M_{\mu\mu}$ and $M_{\pi\pi}$) and BabaYaga (M_{ee}) Monte Carlo code.

should appear as a resonant peak in the invariant mass of lepton or hadron pairs. KLOE investigated both leptonic and hadron decays into pions. Particularly, the hadronic channel allows to increase the sensitivity in the $\rho - \omega$ resonance region because of the U dominant branching fraction into hadrons. The searches for $U \to \mu^+\mu^-, \pi^+\pi^-$ exploited a statistics corresponding to an integrated luminosity of 239.3 pb^{-1} and 1.93 fb^{-1} respectively, and selected events with a small angle Initial State Radiation (ISR) photon [40] and 2 charged tracks with acceptance between 50° and 130°. The application of kinematical cuts and the small angle event selection allowed to reduce the background coming from Final State Radiation (FSR) and ϕ-resonant processes and to increase sensitivity [41] on the dark photon decay. To approach the dielectron mass threshold, the search for $U \to e^+e^-$ has been performed by applying a large angle event selection for both ISR photon and charged leptons ($55° < \theta_{e,\gamma} < 125°$) to a data sample of about 1.5 fb $^{-1}$. Kinematical cuts have been used to remove FSR and resonant backgrounds. To avoid contamination from γ conversion processes in the beam pipe, we asked for events entirely contained within the vacuum pipe ($\rho_{PCA} < 1$ cm, and $|z_{PCA}| < 6$ cm). At the end of the analysis selection the residual background is less then 1%. No significant dark photon signature has been observed and limits at 90% CL have been extracted for all processes on the number of U events by means of the CL_S technique [37–39]. The expected backgrounds have been estimated by a fit to side bands for electron and pion decay channels while for the muon channel a `PHOKHARA` [42] MC generation has been used (see Fig. 3). The limits on U events have then been converted in limits on ε^2 by using the formula reported in Refs. [29–31]. The resulting exclusion limits are shown in Fig. 1 with all other existing limits in the region 0–1000 MeV [25–35]. The $e^+e^-\gamma$ limit excludes some of the remaining $g - 2$ favored region.

4 Higgsstrahlung

The KLOE Collaboration investigated also the Higgsstrahulung process, sensitive to the dark coupling constant α_D and less suppressed with respect previous processes, with an expected cross section up to 1 pb at KLOE. The invisible scenario was considered, where the dark Higgs is lighter then the U boson and escapes detection, in the energy range between the dimuon mass threshold and 1 GeV. In this case, the expected signal is a muon pair from the U-boson decay plus missing energy. The analysis has been performed on two data samples of 1.65 fb^{-1} (collected on the ϕ peak) and 0.2 fb^{-1} collected at E_{cm} = 1000 MeV (off-peak sample) which is not affected by resonant backgrounds (see bottom panel of Fig. 4). In the on-peak analysis the huge background coming from kaon decays (see top panel of Fig. 4) has been reduced thanks to cuts on the quality of the vertex fit. No signal signature has been observed and a Bayesian limit on the number of signal events at 90% CL has been evaluated, bin-by-bin, for the on-peak and off-peak sample separately. Results have been translated in terms of $\alpha_D \times \varepsilon^2$ by using the integrated luminosity information, the signal efficiency, the dark Higgsstrahlung cross section and the branching fraction of the $U \to \mu^+\mu^-$ decay [43]. The combined upper limits [44] projected in the $M_{\mu\mu}$ and M_{miss} directions, for different dark Higgs mass hypotheses and slightly smoothed, are shown in Fig. 5. Values of the order of $10^{-9} \div 10^{-8}$ in $\alpha_D \times \varepsilon^2$ are excluded at 90% CL for a large range of the dark photon and dark Higgs masses. These limits translate in $\varepsilon \sim 10^{-3} - 10^{-4}$ for $\alpha_D = \alpha$ and are in agreement and complementary with BaBar and Belle results [45, 46] as they refer to the same process in a different final state and phase space region.

5 $\gamma\gamma$ physics at KLOE

One of the distinctive features of the KLOE-2 experiment is the possibility to investigate the two photon physics at very low transferred momentum in the space-like region. To distinguish the signal from the huge background coming from ϕ decays and reach the level of precision needed to test the strong QCD dynamic, the study of the interaction between two $\gamma's$ requires to tag the electron and the positron coming from the $e^+e^- \to e^+e^-\gamma^\star\gamma^\star \to e^+e^-X$ process. The leptons are scattered at very small polar angles and X is, a pseudoscalar meson produced by the fusion of the two quasi-real photons. In case of π^0 or η production the photons from the decay have to be detected in the central KLOE detector in association with the HET

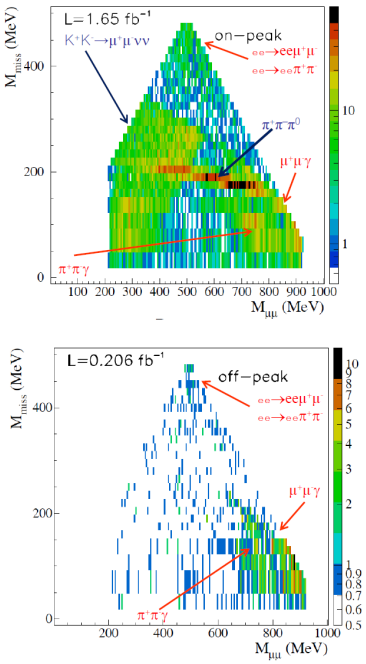

Figure 4. Top panel: $M_{\rm miss}$ Vs $M_{\mu\mu}$ for on-peak sample (1.65 fb^{-1} integrated luminosity). Bottom panel: $M_{\rm miss}$ Vs $M_{\mu\mu}$ for the off-peak sample, (0.2 fb^{-1} integrated luminosity).

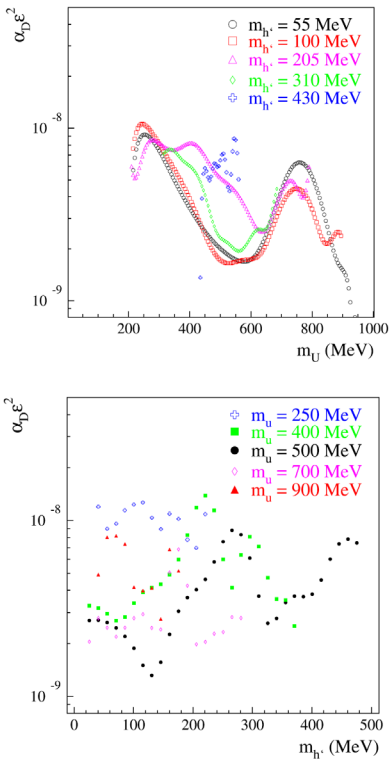

Figure 5. Combined 90% CL upper limits in $\alpha_{\rm D}\times\varepsilon^2$ as a function of $M_{\mu\mu}$ for different values of $m_{\rm h'}$ (top panel) and as a function of $M_{\rm miss}$ for different values of $m_{\rm U}$ (bottom panel).

signal. For this reason two HET stations have been designed and installed just after the bending dipoles (acting like spectrometers) of DAΦNE and are currently operated during the KLOE-2 data taking.

In this section, the most relevant features of the KLOE-2 tagging system operation and the requirements used to classify double arm and single arm events will be presented.

5.1 The HET detector

The HET is a position detector able to measure the deviation of leptons from their main orbit in DAΦNE. The HET stations are placed at the exit of the dipole magnets, 11 m away from the IP, on both the positron and the electron arm. The sensitive area is made up of a set of 28 plastic scintillators (EJ-228), designed for ultra-fast timing and ultra-fast counting applications, with dimensions $(3 \times 5 \times 6)$ mm^3 each. One additional scintillator, of dimensions $(3 \times 50 \times 6)$ mm^3, whose acceptance covers all the others, is used to reinforce evidence for real particles crossing the detector. The light emitted by each of the 28 scintillators is read out through a plastic light guide by a high quantum efficiency photomultiplier (35% for wavelengths between 300 and 400 nm) which matches well the scintillator spectrum. The 28 scintillators are placed at different distances from the beam-line, in such a way that the measurement of the distance between beam and particle can be performed simply knowing which scintillator has been fired. A dedicated DAQ electronic board, based on a Xilinx Virtex-5 FPGA, has been developed for this detector. It provides a MultiHit TDC with a time resolution of 550(1) ps and the possibility to clearly identify the correct bunch crossing ($\Delta T_{\rm bunch}$ = 2.7ns).

5.2 HET operation

The two HET tagger stations have been operated since the very beginning of the KLOE-2 data taking in November 2014. Since KLOE and HET acquisition systems are asynchronous, we use the DAΦNE radiofrequency signal issued once per machine turn, every 325 ns, that is independently recorded by the HET and KLOE, to associate their data. There is a strong evidence that the HET counting rate is almost entirely due to Bhabha scattering events. The hit time structure, indeed, closely reproduces the DAΦNE bunch structure, as can be seen in Fig. 6, while the rate timeline strictly follows the luminosity timeline as measured by the KLOE central detector (KLOEcd). Fig. 7 shows the timelines of the counting rate of the HET stations. The measurement (blu points) are compared with the expectation (red curve) which can be described by the

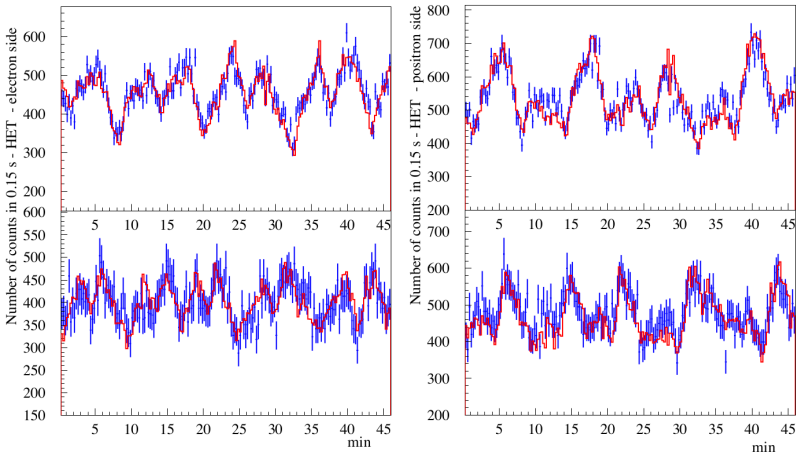

Figure 7. Timelines of the counting rate of the HET stations. The measurements (points with error bars) are compared with the expectation assuming stable DAΦNE operation and a dependence from the Touschek contribution and the luminosity, as obtained from no-collision runs, and the KLOE central detector, respectively. Upper plots are 2015 data and lower are data taken in year 2016. Left plots refer to the electron arm while right plots to the positron side.

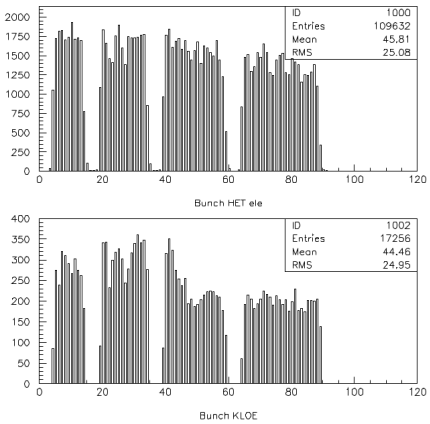

Figure 6. The DAΦNE bunch structure as measured by the electron HET station (upper panel) and by KLOE central detector (lower panel).

following relation:

$$R_{\mathrm{HET_{e,p}}} = \frac{R_{\mathrm{trig}}}{\mathrm{kHz}}(\alpha_{\mathrm{L_{e,p}}}\frac{Lumi}{0.2\mathrm{nb}^{-1}\mathrm{s}^{-1}} + \beta_{\mathrm{e,p}}\frac{I^2_{\mathrm{e,p}}}{A^2}). \qquad (1)$$

R_{trig} is the KLOEcd trigger rate, *Lumi* is the instantaneous luminosity value , $I^2_{\mathrm{e,p}}$ represents the electron or the positron beam currents squared. $\alpha_{\mathrm{L_{e,p}}}$ and $\beta_{\mathrm{e,p}}$ are coefficients (in Hz), normalized to a luminosity of 0.2 $\mathrm{nb}^{-1}\mathrm{s}^{-1}$ and 1 A squared, respectively. Since the HET acquisition system transfers data to the KLOE event-building process only when a valid trigger is asserted by the asynchronous data acquisition system of the KLOEcd, the recorded HET count rate is proportional to the KLOEcd trigger rate and the coefficients of eq. 1 are normalized to the instantaneous trigger rate (in kHz) to take into account such a dependence. In absence of collisions the timeline rate closely follows the approximate I^2 dependence expected for intra-bunch scattering events (Touschek particles). This can be seen in the upper plots of Fig. 8 where the timelines of the counting rate of the HET stations, from a special run operating DAΦNE in no-collision mode in year 2016, are shown. Blue points are measurements while the expectation is represented by the red curve. In the bottom plots the corresponding timelines for the positron and electron circulating currents are reported. The total HET rate is dominated by Bhabha scattering events and is at level of 500-600 kHz. The high counting rates and the fast and reliable feedbacks on machine operation make the HET an ideal luminometer detector as well.

5.3 π^0 search

Data are classified as single arm (SA) double arm (DA) events. The DA data sample has been selected by requiring a time delay between the two stations $\Delta_{\mathrm{e,p}}$ of 18.9 ns corresponding to $|\Delta_{\mathrm{e,p}}| < 7$ bunches. This data sample contains the HET-electron * HET-positron coincidences which are expected, from resolution studies, in a window of ± 1 bunch and a control sample, large enough to characterize the coincidences, with $2 < \Delta_{\mathrm{e,p}} < 7$ bunches. The SA data sample has been selected by choosing:

- events in time with the KLOE trigger, that is a time difference between trigger and clusters $-3 \leq \Delta T_{\mathrm{Trig-clu}} \leq 8$ bunches;
- events in time with a bunch giving two clusters in KLOE with a cluster energy $20 < E_{\mathrm{clu}} < 300$ MeV, with a time delay between the HET station and KLOE within 4 bunches ($|\Delta T_{\mathrm{HET-KLOE}}| < 4$ bunches).

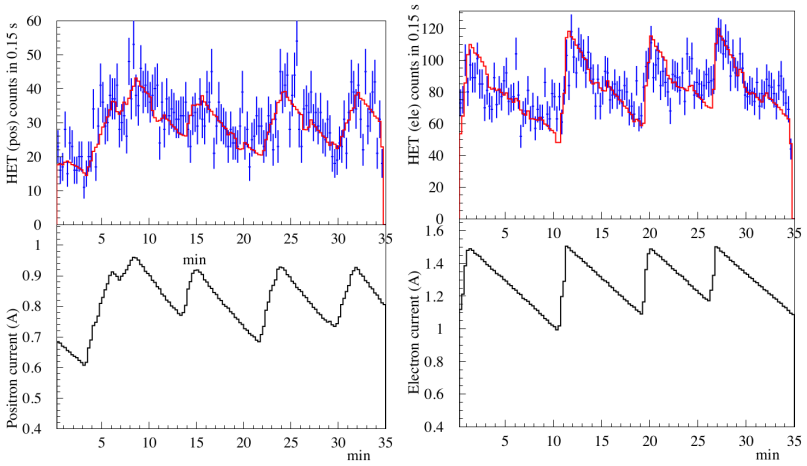

Figure 8. Timelines of the counting rate of the HET stations, from a special run operating DAΦNE in no-collision mode in year 2016. The measurements (points with error bars) are compared with the expectation assuming stable DAΦNE operation and a dependence from the Touschek contribution varying with the square of the circulating current. Bottom panel: timelines of the circulating currents for the same run. The additional peaks in the count rate are due to the KLOE trigger, needed to record HET data. Left plots refer to positron, right plots refer to electrons.

A fine inter-calibration of HET and KLOE TDCs based on bunch structure seen by the KLOE EMC and HET has been applied run by run.

An integrated luminosity of about 500 pb^{-1} has been processed so far, recording information on the hit in the tagger, trigger, DAΦNE operational parameters, clusters and tracks reconstructed in the KLOE central detector. The pre-selected DA sample statistics consists of about 10^8 fully-reconstructed events. The number of $\gamma\gamma$ expected events is predicted by using the *EKHARA* MC generator [47], taking into account the KLOE EMC resolution, in combination with the BDSIM package [48] (GEANT4 application), which allows to track leptons along the machine optics. About 650 events are expected from π^0 decays almost at rest at the current statistics, taking into account detector and trigger efficiency (65%). The analysis of the π^0 candidates requires:

(a) the coincidence between the taggers hits: $|\Delta_{ep}| < 2$ bunches and with the KLOE trigger; two KLOE clusters associated with the same bunch with $\Delta T_{\mathrm{KLOE_{clu}-HET}} \leq 4$ bunches and with energy $E_\gamma < 300$ MeV (see blue curve in Fig. 9)

(b) $E_\gamma > 20$ MeV (see black curve in Fig. 9)

(c) $30 < E_\gamma < 135$ MeV (see green curve in Fig. 9)

(d) $P_{\pi^0} < 90$ MeV; $\cos\alpha_{\gamma\gamma} < -0.8$;
$80 < M_{\gamma\gamma} < 230$ MeV; $|\Delta T - \Delta R/c| < 1.1$ ns (see red curve in Fig. 9)

Figure 9 shows the distribution of the total energy of the photon pairs at different stages of the π^0 selection, the distribution in red is obtained by applying the constraints suggested by EKHARA and BDSIM simulation (see point (d) above) taking into account of the detector resolution. The

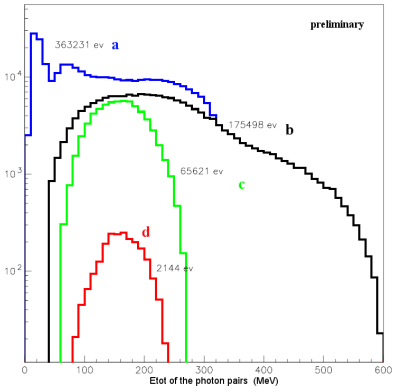

Figure 9. Distributions of the total energy of the photon pairs for samples satisfying different criteria as described in the text. The distribution in red is obtained from events within the ranges indicated by EKHARA and BDSIM simulations.

background evaluation is performed on a run-by-run basis. We select as background the events out of the HET coincidence window which we use in this study together with HET events that can not be in time with the KLOE trigger. The sample is dominated by random coincidences between HET and KLOE detector even at the end of the π^0 selection. Techniques to separate the random coincidences from π^0 signal are still in progress.

Conclusions

The KLOE Collaboration investigated the existence of the dark photon in the prompt and visibly-decay hypothesis,

by means of the $\phi-$Dalitz decay, continuum processes and Higgsstrahlung. No signal has been found and stringent limits have been extracted below 1 GeV, constraining the $g-2$ favored region. A new run, with the KLOE-2 upgraded detector has started in November 2014 to record 5 fbˆ−1 within March 2018. The expected larger new statistical sample and the KLOE-2 inner tracking detector, which allows a better vertex reconstruction and a higher invariant mass resolution, will improve the current sensitivity on dark photon signal of a factor of about 2. Moreover, new searches for invisible dark photon decays into light DM states and for a leptophobic B boson are also planned. KLOE-2 aims also to perform the precision measurement (1% level) of the π^0 width which allows to test the strong QCD dynamics. For this reason two high energy taggers have been installed in the DAΦNE layout and are currently operated during the KLOE-2 data taking. The two HET stations are completely noiseless and the timelines of the counting rate for electron and positron stations show only two visible contributions from luminosity and from Touschek The total rate is dominated by the Bhabha scattering and is at the level of 500-600 kHz. These characteristics allow to have fast and reliable feed-backs on the machine operation making the HET a luminometer detector as well. We have pre-filtered candidates of single-π^0 production from $\gamma\gamma$ scattering. A total integrated luminosity of about 500 pb^{-1} of DA and SA data are being currently analyzed.

References

[1] B. Holdom, Phys. Lett. B **166**, 196 (1985)
[2] C. Boehm and P. Fayet, Nucl. Phys. B **683**, 219 (2004)
[3] P. Fayet, Phys. Rev. D **75**, 115017 (2007)
[4] Y. Mambrini, J. Cosmol. Astropart. Phys. **1009**, 022 (2010)
[5] M. Pospelov, A. Ritz and M.B. Voloshin, Phys. Lett. B **662**, 53 (2008)
[6] O. Adriani et al., Nature **458**, 607 (2009)
[7] M. Aguilar et al., Phys. Rev. Lett. **110**, 141102 (2013)
[8] P. Jean et al., Astronomy Astrophysics **407**, L55 (2003)
[9] J. Chang et al., Nature **456**, 362 (2008)
[10] F. Aharonian et al., Phys. Rev. Lett. **101**, 261104 (2008)
[11] A. A. Abdo et al., Phys. Rev. Lett. **102**, 181101 (2009)
[12] R. Barnabei et al., Eur. Phys. J. C **56**, 333 (2008)
[13] M. Pospelov, Phys. Rev. D **80**, 095002 (2009)
[14] K. Kampf, B. Moussallam, Phys. Rev. D **79**, 076005 (2009)
[15] J. Bijnens, K. Kampf, Nucl. Phys. B, Proc. Suppl. 207-208, 220-223 (2010)
[16] K. Nakamura, J. Phys. G **37**, 075021 (2010) (controllare quello 2012)
[17] H. Primakoff, Phys. Rev. **81**, 899 (1951)
[18] D. Babusci et al., Eur. Phys. J. C **72**, 1917 (2012)
[19] M. Adinolfi, et al., Nucl. Instrum. Meth. A **488**, 51 (2002)
[20] M. Adinolfi, et al., Nucl. Instrum. Meth. A **482**, 364 (2002)
[21] Bencivenni G., Domenici D., Nucl. Instrum. Meth. A, **581**, 581 (2007); Di Cicco A. and Morello G., Acta Phys. Pol. B, **46**, 73 (2015)
[22] Happacher F. and Martini M., Acta Phys. Pol. B, **46**, 87 (2015)
[23] Babusci D. et al., Acta Phys. Pol. B, **46**, 87 (2015)
[24] Babusci D. et al., Acta Phys. Pol. B, **46**, 81 (2015)
[25] H. Merkel et al., Phys. Rev. Lett. **112**, 221802 (2004)
[26] S. Abrahamyan et al., Phys. Rev. Lett. **107**, 191804 (2011)
[27] F. Archilli et al. Phys. Lett. B **706**, 251 (2012)
[28] D. Babusci et al., Phys. Lett. B **720**, 111 (2013)
[29] D. Babusci et al., Phys. Lett. B . **736**, 459 (2014)
[30] A. Anastasi et al., Phys. Lett. B **750**, 633 (2015)
[31] A. Anastasi et al., Phys. Lett .B **757**, 356 (2016)
[32] P. Adlarson et al., Phys. Lett. B **726**, 187 (2013)
[33] G. Agakishiev et al., Phys. Lett. B **731**, 265 (2014)
[34] J. P. Lees, Phys. Rev. Lett. **113**, 191804 (2014)
[35] J.R. Batley et al., Phys. Lett. B **746**, (2015)
[36] M. Reece and L. T. Wang, JHEP **0907**, 051 (2009)
[37] G. J. Feldman and R. D. Cousins, Phys. Rev. D **57**, 3873 (1998)
[38] T. Junk, Nucl. Instr. Meth. A **434**, 435 (1999)
[39] A. L. Read, J. Phys. G: Nucl. Part. Phys. **28**, 2693 (2002)
[40] D. Babusci et al., Phys. Lett. B **720**, 336 (2013)
[41] L. Barzè et al., Eur. Phys. J. C **71**, 1680 (2011)
[42] H. Czyż, A. Grzelinsk, J. H. Kühn and G. Rodrigo Eur. Phys. J. C **39**, 411 (2005)
[43] B. Batell et al., Phys. Rev. D **79**, 11508 (2009)
[44] A. Anastatsi et al., Phys. Lett. B **747**, 365 (2015)
[45] J. P. Lees et al., Phys. Rev. Lett. **108**, 211801 (2012)
[46] I. Jaegle et al., Phys. Rev. Lett. **114**, 211801 (2015)
[47] H. Czyz, S. Ivashyn, Comput. Phys. Commun. **182**, 1338 (2011)
[48] I. Agapov, G.A. Blair, S. Malton, L. Deacon, Nucl. Instrum. Meth. A **606**, 708 (2009)